Low-lying resonant states in ^{16}F using a ^{15}O radioactive ion beam

D. W. Lee,[1,2,*] K. Peräjärvi,[1,†] J. Powell,[1,3] J. P. O'Neil,[3] D. M. Moltz,[4] V. Z. Goldberg,[5] and Joseph Cerny[1,4]

[1]*Nuclear Science Division, Lawrence Berkeley National Laboratory, Berkeley, California 94720, USA*

[2]*Department of Nuclear Engineering, University of California, Berkeley, California 94720, USA*

[3]*Life Sciences Division, Lawrence Berkeley National Laboratory, Berkeley, California 94720, USA*

[4]*Department of Chemistry, University of California, Berkeley, California 94720, USA*

[5]*Texas A&M University, Cyclotron Institute, College Station, Texas 77843, USA*

(Received 30 January 2007; published 20 August 2007)

A 120 MeV ^{15}O radioactive ion beam with an intensity on target of 4.5×10^4 pps has been developed at the 88-Inch Cyclotron at the Lawrence Berkeley National Laboratory. This beam has been used to study the level structure of ^{16}F at low energies via the $p(^{15}\mathrm{O}, p)$ reaction using the thick target inverse kinematics method on a polyethylene target. The experimental excitation function was analyzed using R-matrix calculations. Significantly improved values for the level widths of the four low-lying states in ^{16}F are reported. Good agreement with the theoretical spectroscopic factors is also obtained.

DOI: 10.1103/PhysRevC.76.024314 PACS number(s): 27.20.+n, 25.40.Cm, 25.60.Bx, 21.10.Dr

I. INTRODUCTION

Among the nuclei in the $A = 16, T = 1$ isobaric triad, many states in ^{16}N and ^{16}O have been well established, but less has been reported on ^{16}F. Four states of ^{16}F below 1 MeV have been identified experimentally, and their energies are currently known to an accuracy of 4–6 keV (the next known state of ^{16}F lies at 3.76 MeV) [1]. Experimental studies with stable beams have also established spin-parity values for these low-lying states, but only upper limits or rough estimates of their level widths have been reported. The main difficulty in characterizing ^{16}F has been that it can be broadly studied by relatively few reactions, primarily $^{14}\mathrm{N}(^3\mathrm{He},n)$ [2–4], $^{16}\mathrm{O}(^3\mathrm{He}, t)$ [5–8], $^{16}\mathrm{O}(p, n)$ [9–13], and $^{19}\mathrm{F}(^3\mathrm{He}, ^6\mathrm{He})$ [6]. Another difficulty in determining level widths is that these transfer reactions typically only provide energies and spin-parity values.

All the states in ^{16}F are unbound to $^{15}\mathrm{O}+p$. The spins and parities of the low-lying states have been found to be $0^-, 1^-, 2^-$, and 3^- in ascending order in energy, and are believed to have ^{15}O core-single proton configurations, namely, $1p_{1/2}^{-1}2s_{1/2}$ for the $0^-, 1^-$ states and $1p_{1/2}^{-1}1d_{5/2}$ for the $2^-, 3^-$ states [7,10]. However, the variation in the $1d_{5/2} - 2s_{1/2}$ energy level difference across the members of the $A = 16, T = 1$ isobaric triad [14,15] made initial ^{16}F spin assignments uncertain [2,4] since ^{16}N showed $J^\pi = 2^-, 0^-, 3^-, 1^-$ for the four levels in ascending energy order while $J^\pi = 0^-, 2^-, 1^-, 3^-$ arose in ^{16}O, as is shown in Fig. 1.

A recently developed ^{15}O radioactive ion beam from the BEARS (Berkeley Experiments with Accelerated Radioactive Species) facility [16–18] at the Lawrence Berkeley National Laboratory (LBNL) has been used to study the structure of ^{16}F using $^{15}\mathrm{O}+p$ elastic resonance scattering and the thick target inverse kinematics (TTIK) method on a polyethylene target [19,20]. Of particular interest is establishing the level widths of the low-lying ^{16}F states, which can be compared to theoretical calculation for this proton unbound nucleus.

II. EXPERIMENT

The BEARS facility at LBNL's 88-Inch Cyclotron provides several proton-rich radioactive ion beams for studies of exotic nuclei and nuclear astrophysics [18,21]. Radioactive isotopes such as ^{11}C ($T_{1/2} = 20.26$ min) and ^{14}O ($T_{1/2} = 71$ sec) have been produced by bombarding 40 μA of 10 MeV protons from LBNL's Life Sciences Division's medical cyclotron onto a nitrogen gas target via $^{14}\mathrm{N}(p, \alpha)$ and $^{14}\mathrm{N}(p, n)$ reactions, respectively. These isotopes are then transferred in the form of volatile carbon dioxide ($^{11}CO_2$ for ^{11}C, and $[^{14}\mathrm{O}]CO_2$ for ^{14}O) 350 m via a capillary line to the 88-Inch Cyclotron for injection into its Advanced Electron Cyclotron Resonance (AECR) ion source. Recently, an ^{15}O beam ($T_{1/2} = 122$ sec) has been developed as the third radioactive ion beam in the BEARS system based on the process developed for the ^{14}O beam. The nuclide ^{14}O is produced in the form of $H_2{}^{14}\mathrm{O}$ by adding a small amount of hydrogen to the nitrogen gas target, and this is then chemically converted in two rapid steps to $[^{14}\mathrm{O}]CO_2$ [17]. For the case of ^{15}O production, the gas target was loaded with $^{15}N_2$ instead of $^{14}N_2$. $H_2{}^{15}\mathrm{O}$ was formed inside the gas target cell and chemically converted to $[^{15}\mathrm{O}]CO_2$ for transfer to the 88-Inch Cyclotron. In addition, to conserve the $^{15}N_2$ gas using this batch type production process, it was stored and recycled into the gas target [22].

To set up the beam optics and eliminate the ^{15}N component of the beam, a 160 MeV $^{20}\mathrm{Ne}^{8+}$ beam was initially used as a pilot beam; then a weak 120 MeV ^{15}N beam was tuned into the experimental area, since the $^{15}\mathrm{N}^{6+}$ accelerating frequency is very close to that of the $^{20}\mathrm{Ne}^{8+}$. Next, the ^{15}N beam was fully stripped to its 7^+ charge state by passing it through a thin aluminum stripper foil placed before an analysis magnet. The subsequent beam optics was then adjusted to focus the $^{15}\mathrm{N}^{7+}$ beam on the target. These adjustments were then

*dwlee@lbl.gov

†Present address: Radiation and Nuclear Safety Authority, Helsinki, Finland.

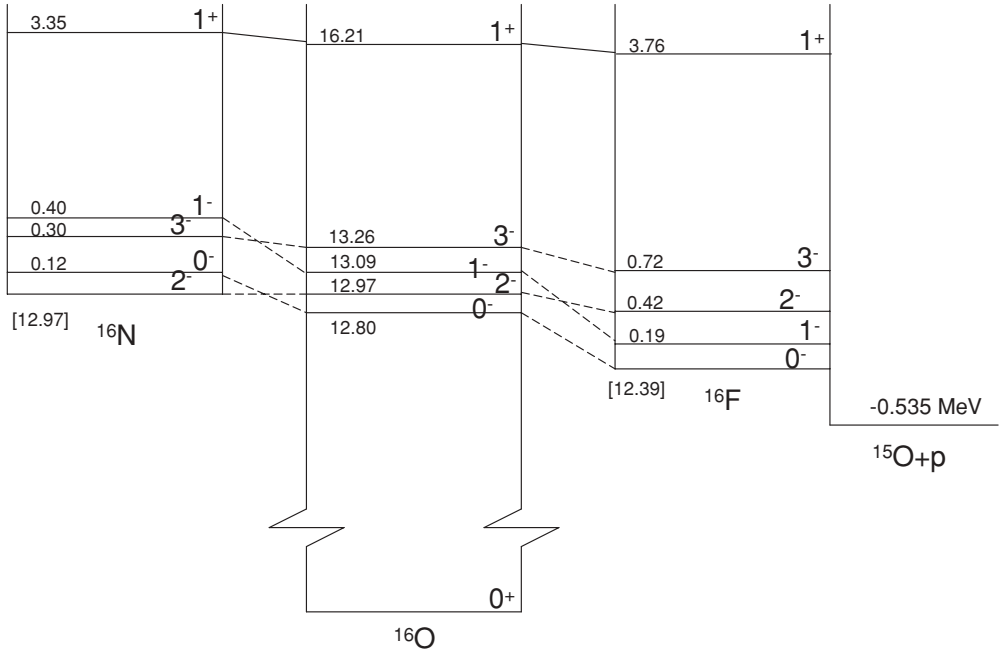

FIG. 1. An isobaric energy level diagram for the $A = 16$, $T = 1$ nuclear states [1].

changed to obtain $^{15}O^{8+}$ from an accelerated and stripped $^{15}O^{6+}$ beam. Finally, the cyclotron was carefully tuned to maximize a focused 120 MeV $^{15}O^{8+}$ beam on the target position, eliminating ^{15}N contamination as much as was possible. However, the cyclotron frequency difference between $^{15}N^{6+}$ and $^{15}O^{6+}$ is so small (1.2 kHz) that a residual amount of ^{15}N contamination was still observed in the low energy region of the ^{15}O spectrum. The measured amount of ^{15}N contamination of the ^{15}O beam was less than 2% throughout the experiment. The ^{15}O beam profile measured at 0° in the laboratory using a single silicon detector (see below) is shown in Fig. 2.

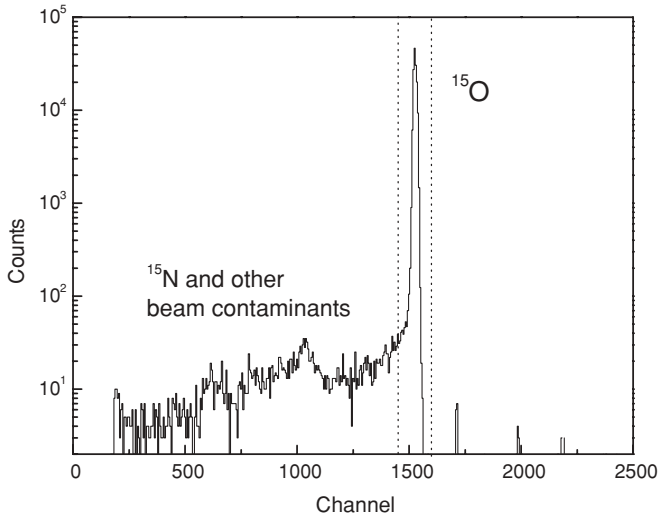

FIG. 2. The observed ^{15}O beam profile at 0° in the laboratory without a Ni degrader and a target. A small tail consisting of ^{15}N and other beam contaminants is observed. See text.

Figure 3 shows the last stage of the experimental setup. At the beginning of the experiment, the ^{15}O beam was counted at 0° with a single silicon detector (1000 μm), and scattered ^{15}O beam from a thin gold foil was measured simultaneously by a ΔE-E monitor telescope (25 μm and 300 μm, respectively) placed at 20° to the beam axis. The ratio between these two measurements allowed us to calculate that the average beam intensity of ^{15}O impinging on the target was 4.5×10^4 pps. The beam energy spread was measured to be 1.66 MeV FWHM (the size of the beam spot was about 7 mm in diameter) at 0° after going through the aluminum stripper foil and the gold scattering foil (see Fig. 3). Data from the ΔE-E monitor telescope were recorded throughout the run.

For the $^{15}O + p$ experiment, the 120 MeV ^{15}O beam[1] was slowed down by a 3.81 μm Ni degrader, and completely stopped in a thick 200 μm (18.4 mg/cm^2) CH_2 target. The thickness of Ni degrader was chosen to stop the ^{15}O beam very close to the end of the target, minimizing the energy loss of emerging low energy protons within the CH_2 target. The main particle telescope was composed of ΔE(30 μm), $E1$(700 μm), and $E2$(5000 μm) silicon detectors, located behind a circular collimator at 0° at a distance of 10.9 cm from the target. The first two detectors were thick enough to detect protons from the four low-lying resonance states in ^{16}F, and the third one permitted the detection of high energy protons of up to 7 MeV in the center-of-mass (c.m.). The total energy resolution was found to be 28 keV in the center of mass (c.m.) (FWHM) for the energy region below 3 MeV c.m. The major contributions are found to be 24 keV from the energy resolution of the

[1]This beam energy was chosen to permit maximum ^{15}O production by extracting the 6^+ charge state from the AECR ion source, which has the maximum yield.

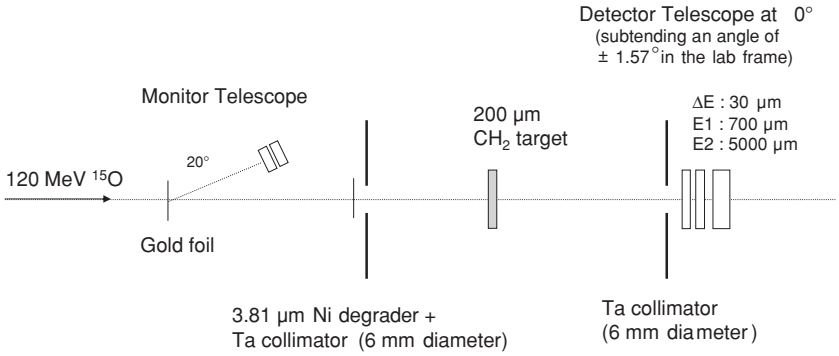

FIG. 3. The experimental setup for the ^{15}O+p resonance scattering reaction. See text.

detection system (detectors and electronics), 12 keV from the beam spread [23] and the proton energy straggling [24] in the CH_2 target, and 6 keV from the angular spread due to detector geometry and beam optics [25].

Figure 4 shows a typical two-dimensional particle identification spectrum recorded during the experiment using the ΔE-$E1$ part of the detector telescope. The proton band is clearly shown in this figure along with a lot of β^+ counts. A gate was drawn around this proton band, and the proton spectrum inside the gate was converted into a one-dimensional excitation function. This excitation function consisted of the sum of the ΔE and $E1$ detectors up to 2.7 MeV c.m. (see Fig. 4 caption) and at higher energies was the sum of the ΔE, $E1$, and $E2$ detectors (in triple coincidence). The energy calibration for the ΔE-$E1$ and the ΔE-$E1$-$E2$ detector system was established by using the $p(^{15}N, p)$ reaction [26–29] before and after the main $p(^{15}O, p)$ measurement because the energy levels of the relevant excited states in ^{16}O are well known. The measured laboratory energy of the protons at a given laboratory angle can then be converted to center-of-mass energy by using

$$E_{\text{c.m.}} = \frac{m_p + M(^{15}\text{O})}{4M(^{15}\text{O})\cos^2\vartheta_{\text{lab}}} E_{p,\text{lab.}}. \tag{1}$$

Finally, the proton counts were converted into cross sections without any background subtraction, so that an arbitrary cross-section unit has been used for the excitation function. The experimental cross section, $\frac{d\sigma}{d\Omega}$, was calculated by using an energy-dependent target thickness, Δx, which is inversely proportional to the stopping power, $\frac{dE}{dx}$ [25]:

$$\frac{d\sigma}{d\Omega} = \frac{R}{\rho \times \Delta x \times I \times \Delta\Omega} = \frac{R}{\rho \times \left(\Delta E \times \frac{dx}{dE}\right) \times I \times \Delta\Omega}, \tag{2}$$

where R is the proton yield, ρ is the target density [atoms/cm^3], $\Delta\Omega$ is the detector solid angle, and I is the time integrated ^{15}O beam intensity [30,31].

Figure 5 shows our measured $p(^{15}\text{N}, p)$ excitation function along with the results from the two previous $^{15}\text{N}(p, p)$ studies [27,29]. Also shown are the ^{16}O resonance states used for the energy calibration. A second order polynomial was used for the energy calibration, but the nonlinearity is less than 3% compared to a linear calibration. The uncertainty of our energy calibration was estimated to be about ±15 keV in the center-of-mass frame. Figure 6 then shows the $p(^{15}\text{O}, p)$ excitation function up to 6.5 MeV, measured at 180° c.m. using the data from the complete detector telescope (ΔE, $E1$, $E2$) as described earlier.

III. DATA ANALYSIS

In this study, the level widths of the first four states in ^{16}F were the main focus of the data analysis, so that only the

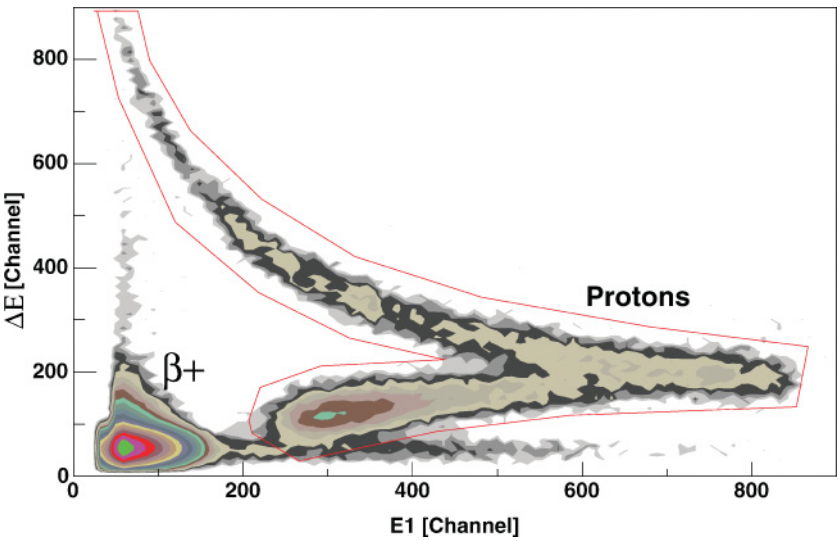

FIG. 4. (Color online) A typical two-dimensional particle identification spectrum for ΔE-$E1$ coincidences. Protons with energies below 2.7 MeV c.m. (around channel number 850 in $E1$) stopped in the ΔE-$E1$ detector telescope. Protons above this energy punched through the $E1$ detector and were also recorded in coincidence in the $E2$ detector. Consequently, the deposited energy in both the ΔE and the $E1$ detectors starts decreasing after this point, as is shown. See text.

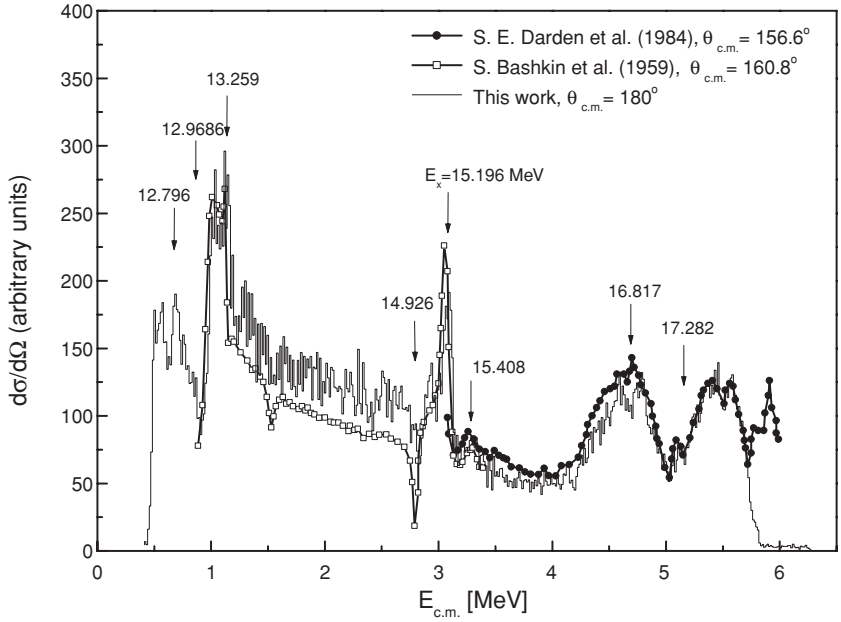

FIG. 5. The measured ^{15}N+p excitation function at 180° c.m. without background subtraction used for the energy calibration. ^{16}O resonance states used in the energy calibration are indicated. Experimental results from previous studies at different c.m. angles are also shown.

low energy region below 3 MeV in the center-of-mass was selected for R-matrix analysis. As shown in Fig. 7, the first four states in ^{16}F are quite distinguishable, and the interference between potential and resonance scattering is clearly observed. In order to compare these experimental results with theory, a resonance scattering analysis code, which is based on the R-matrix equations in Refs. [32,33], was written to calculate the theoretical excitation function. In order to perform the correct comparison with theory, background subtraction is necessary because protons from the reaction between the ^{15}O beam and ^{12}C in the CH_2 target may contribute to the measured proton spectrum. Due to the limited beam time, we did not measure the ^{12}C(^{15}O,p) spectrum. As a result, the earlier ^{12}C(^{14}O,p) reaction data using 120 MeV ^{14}O were used to estimate this background contribution [18][2]. This background proton spectrum is also shown in Fig. 7, and the background is small in the region of the four low-lying resonances.

The J^π values of these four states are 0^-, 1^-, 2^-, and 3^- (as discussed earlier). To make the analysis simple, the 0^- and 1^- states are assumed to be pure $1p_{1/2}^{-1}2s_{1/2}$ configurations, and

[2]These earlier ^{14}O+^{12}C data showed broad feature-less proton background spectra. Since the ^{15}O+^{12}C reaction has comparable kinematics over the proton energy range of interest, we expect comparable background spectra.

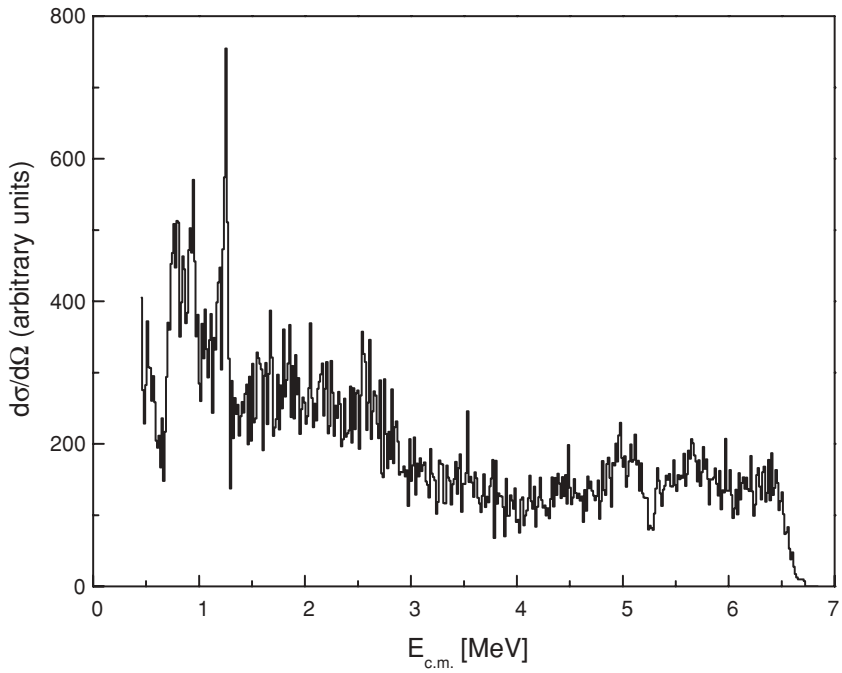

FIG. 6. The measured ^{15}O+p excitation function at 180° c.m. up to 6.5 MeV c.m.

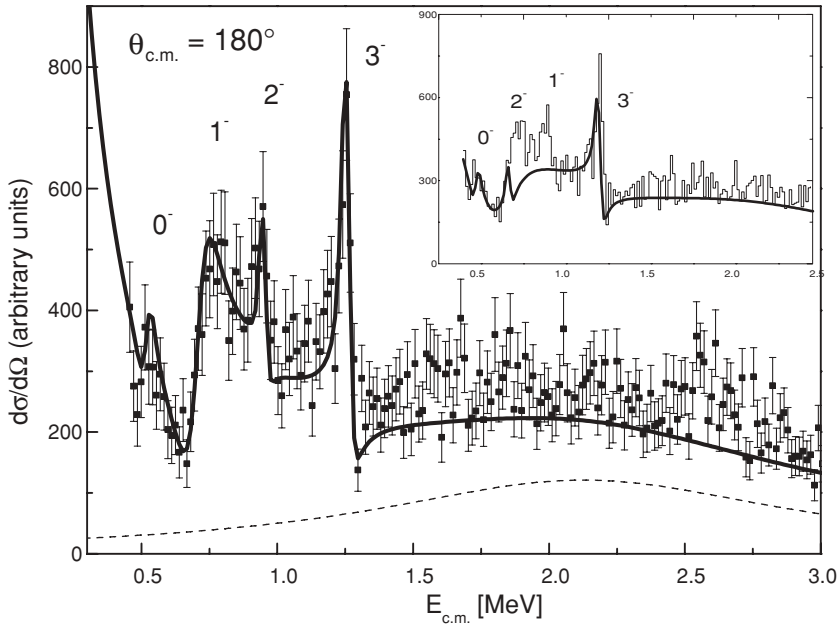

FIG. 7. The R-matrix fit for the low-lying states in ^{16}F. The solid line represents the R-matrix calculation added to the background; the background function is shown as a dashed line. See text for details. The inset shows the best R-matrix fit, assuming a spin order of 0^-, 2^-, 1^-, and 3^- for the low-lying states. It is clear that this spin order is unable to reproduce the measured data.

only s-wave contributions to these resonances are considered. For the 2^- and 3^- states, only d-wave contributions are considered with a $1p_{1/2}^{-1}1d_{5/2}$ configuration. Theoretical shell model calculations predict that the amplitudes of these simple configurations are well over 0.97 in these states (see Table III in Ref. [10] and Table IV in Ref. [7]). The partial width of each combination of channel spin, s, and orbital angular momentum, ℓ, is represented as $\Gamma_{s\ell}$, which is a key parameter in the data fitting.

For the data fitting, the R-matrix calculation was convoluted with the experimental resolution function, and compared to the experimental cross section, after adding the background function discussed earlier whose shape was adopted from an earlier ^{12}C(^{14}O,p) experiment. All the fitting parameters in both the R-matrix analysis (E_R and $\Gamma_{s\ell}$) and the background function (a simple Gaussian function) were iterated using a minimization algorithm, MINUIT [34], until the lowest chi-square per degree of freedom was obtained. This procedure was repeated, changing the initial values, upper/lower limits, and step sizes of the fitting parameters, until the best χ^2 value was obtained. In addition, a 50% uncertainty in the amplitude of the background function is also taken into account in the chi-square analysis.

A channel radius of 5 fm obtained by the conventional formula $r = 1.45(A_1^{1/3} + A_2^{1/3})$ fm was used in all the final R-matrix calculations. Different values for the channel radius within a range from 4.5–5.5 fm were also tested, but no significant change in the results was observed. We also included high-lying resonances in our R-matrix calculation, but we could not find any significant effect from those. Finally, the level width and excitation energy of each state were obtained from the average value of these fitting results; the average χ^2 value was 1.08 per degree of freedom, which varied from 0.84 to 1.27.

IV. RESULTS AND DISCUSSION

The experimental cross section and the R-matrix calculations are shown in Fig. 7, where the adopted background function is also shown. The level widths and excitation energies of the four states in this study are summarized in Table I. Figure 8 shows variations of the chi-square value as a function of the level width for each state. These were calculated by varying the level width of one state to obtain $\Delta\chi^2$ while keeping the other parameters fixed at their optimized values.

TABLE I. A comparison of previous experimental studies with our results for the level widths.

Compilation [1]			^{14}N(^{3}He, n)^{16}F [2]		^{14}N(^{3}He, n)^{16}F(p)^{15}O [4]		^{16}O(^{3}He, t)^{16}F [7]		p(^{15}O, p)[a]		
E_x [MeV ± keV]	J^π	Γ_p [keV]	J^π	Γ_p [keV]	J^π	Γ_p [keV]	J^π	Γ_p [keV]	E_x[b] [MeV ± keV]	J^π	Γ_p [keV][c]
0	0^-	40 ± 20	0^-	50 ± 30	1^-	39 ± 20	0^-	≈25	0	0^-	22.8 ± 14.4
0.193 ± 6	1^-	<40	2^-	<40	0^-	96 ± 20	1^-	≈100	0.187 ± 18	1^-	103 ± 12
0.424 ± 5	2^-	40 ± 30	1^-	40 ± 30	⩾2	24 ± 20	2^-		0.416 ± 20	2^-	4.0 ± 2.5
0.721 ± 4	3^-	<15	3^-	<15	⩾2	24 ± 20	3^-		0.722 ± 16	3^-	15.1 ± 6.7

[a]This work.
[b]The uncertainty primarily comes from the energy calibration (±15 keV).
[c]95% confidence level.

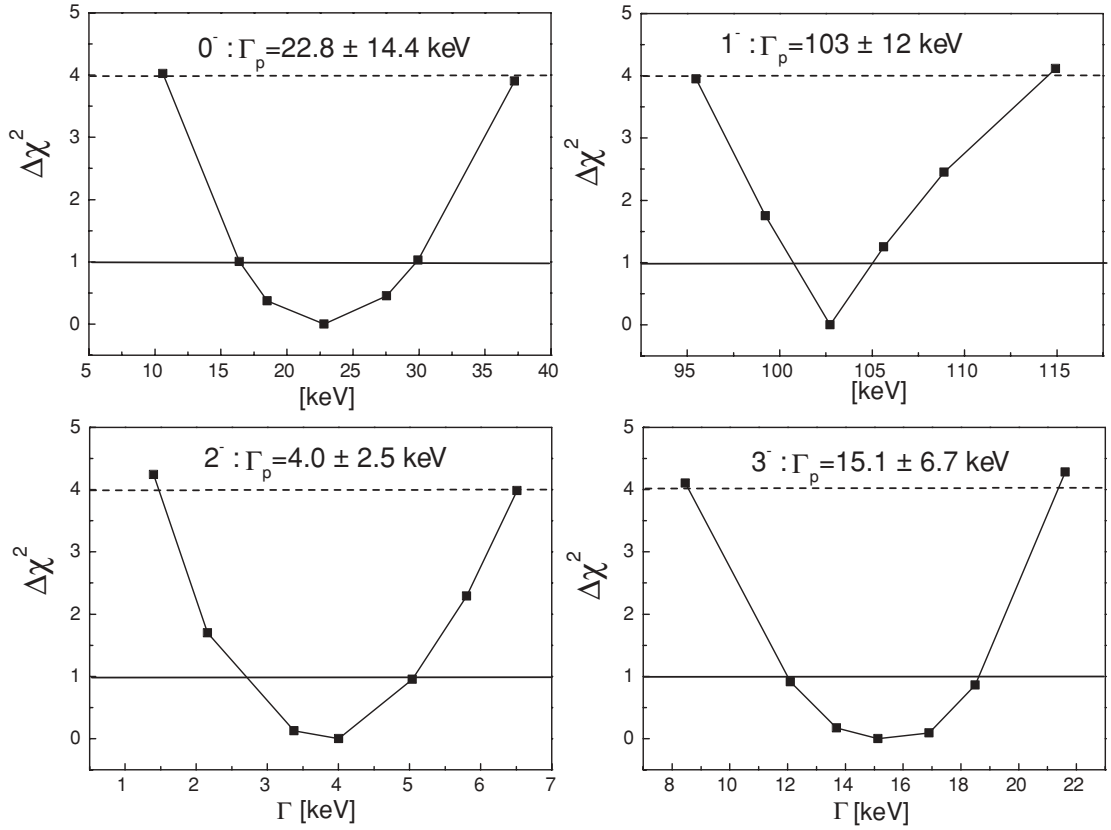

FIG. 8. The variations in the chi-square value as a function of level width. A confidence level of 95% is represented by the dotted lines ($\Delta\chi^2 = 4$), and 68.3% by the solid lines ($\Delta\chi^2 = 1$). See text.

The uncertainty of each level width was then determined by its value at $\Delta\chi^2$ equal to 4, which corresponds to a confidence level of 95%[3]. Spin-parity assignments were not tested in this work because data were only taken at one angle, but a different order of J^π values such as 0^-, 2^-, 1^-, and 3^- for the first four states in ^{16}F was found to create an excitation function whose χ^2 value was unacceptable (see the inset of Fig. 7). The excitation energies of these four states were also fitting parameters, and the results are in very good agreement with the known values [1]. However, no improvement in the values was possible since these values are already known quite accurately with uncertainties less than 10 keV.

The level widths in Table I obtained from the ^{15}O+p data show several different results when compared with the compiled values from the previous studies. The level widths of the 0^- and 1^- states were reported to be 40 ± 20 keV and less than 40 keV, respectively, in Ref. [1]. Our study finds that the 0^- state has a level width of 22.8 ± 14.4 keV, and that the broader 1^- state has a width of 103 ± 12 keV (about twice the compiled value). However, the ^{14}N(^{3}He, n)^{16}F data [4] reported that the first two states are 1^- and 0^- with level widths of 39± 20 keV and 96 ± 20 keV respectively (see Table I). Also note that the ^{16}O(^{3}He, tp) data [7] reported similar results (to ours) of ∼25 keV and ∼100 keV for the 0^- and 1^- state, respectively. The level width of the 2^- state is found to be 4.0± 2.5 keV which is much narrower than the compiled value of 40 ± 30 keV, while 15.1 ± 6.7 keV for the 3^- state is in good agreement with <15 keV in Ref. [1]. As reflected in the experimental results, the 0^- and 1^- states show relatively broad peaks as would be expected from s-wave scattering compared to the narrower 2^- and 3^- states from the d-wave scattering.

In order to compare these experimental level widths to theoretical expectations, the single particle width of each state,Γ_{sp}, was obtained from a Woods-Saxon potential model calculation using two different diffusion parameters, a, as is shown in Table II (also see Table III). The first, the conventional calculation, had the radius parameter $r_0 = 1.2$ fm and the diffuseness parameter, $a = 0.65$ fm; the second, more diffuse potential had a smaller radius, which was compensated by a larger $a = 0.75$ fm. Then the well depths of the potentials were fixed by a fit to the excitation energies of the levels in ^{16}N, and the same parameters were used to calculate the excitation energies of the levels in ^{16}F. The only new factors in the calculations for ^{16}F were a small change of the reduced mass and the Coulomb potential of the uniformly charged sphere with radius parameter, r_C, of 1.2 fm. (The change of this parameter to 1.17 fm resulted in ∼10 keV shift toward less binding.)

The "conventional" parameters in Table II result in a ^{16}F ground state binding energy of −0.577 MeV, which is smaller

[3]In cases where the $\Delta\chi^2$ values are asymmetric for$\Delta\chi^2 = 4$ (e.g., the 1^- level), the larger value is used.

TABLE II. Woods-Saxon potential model parameters.

	Parameter set #1		Parameter set #2	
	0^-	1^-	0^-	1^-
V	−55.36 MeV	−54.42 MeV	−55.474 MeV	−54.455 MeV
r_o	1.2 fm	1.2 fm	1.17 fm	1.17 fm
a	0.65 fm	0.65 fm	0.75 fm	0.75 fm
r_c	1.2 fm	1.2 fm	1.2 fm	1.2 fm
V_{so}	7.64 MeV	7.64 MeV	7.64 MeV	7.64 MeV
a_{so}	0.65 fm	0.65 fm	0.65 fm	0.65 fm
$r_{o\,so}$	1.17 fm	1.17 fm	1.17 fm	1.17 fm

than the experimental value of −0.535 MeV. We consider this disagreement as evidence of a need for a change of the parameters, which were fixed for stable nuclei (see also Ref. [35]). Use of the diffuse potential provides 42 keV more binding than experiment for the 0^- state and 58 keV more than for the 1^- state (535 keV +193 keV). In this case we can consider the differences as an indication that the spectroscopic factors of these states are less than the single particle limit. To estimate the needed changes of the spectroscopic factors, we took the ratio of the differences between the calculated and experimental level positions to the average difference between the excitation energies of the $2s_{1/2}$ states (0^- and 1^-) and the $1d_{5/2}$ states (2^- and 3^-) in ^{16}N and ^{16}F. As a result, we obtained 0.91 for the spectroscopic factor of the 0^- state, and 0.88 for the 1^- state (see Table III).

This single particle width calculation allows us to estimate the proton partial width of each state using the equation $\Gamma_p = C^2S\Gamma_{sp}$ if we know the single-particle spectroscopic factor, C^2S. Experimental spectroscopic factors for ^{16}N, which has the same core-single particle configuration as ^{16}F, are available from a ^{15}N$(d, p)^{16}$N transfer reaction study [36]. However, they are a factor of two less than theoretical prediction and this discrepancy has not been clearly explained (see discussion in Ref. [36]). Theoretical spectroscopic factors for the analog states in ^{16}N [37] are given in Table III for comparison.

As can be seen in Table III, the widths of all four levels are close to the single particle shell model predictions with either of the two diffusion parameters. This successful single particle approach was then applied to the level shifts between the mirror nuclei. We wanted to calculate the shifts with two goals: (1) to understand how the general features of the potential affect the isotopic shift for the s-states in ^{16}N and ^{16}F, and (2) to obtain an additional estimate of the single particle spectroscopic factors for the s-states. The isotopic shift of the levels depends primarily on the global radial distribution of the wave functions in the Coulomb field. It is well known [38–40] that the shift (to stronger binding) in the proton-rich nuclide is greatest for s-states due to the greater spatial extent of their wave functions.

The absolute values of the spectroscopic factors are dependent upon the excitation energies of the $1d_{5/2}$ states in our approach. These excitation energies in their turn are dependent upon electromagnetic corrections and details of their nuclear structure (one can consider mixing with the nearest $d_{3/2}$ states, for example). These corrections could be as large as 100 keV, which would result in 2% corrections to the absolute values of the spectroscopic factors. In addition, the differences in the values of the spectroscopic factors for the 0^- and 1^- states can have physical meaning. The smaller spectroscopic factor for the 1^- state can be related to a possible admixture of the $1p_{1/2}^{-1}1d_{3/2}$ configuration (it is much more difficult to find a possible admixture for the $J^\pi = 0^-$).

In conclusion, the experimental data on the widths and the excitation energies of the lowest states in ^{16}F favor the more diffuse nuclear potential, as was observed earlier for the ^{15}F case [35]. The four low-lying states of ^{16}F manifest remarkably clear single particle structure. In this sense the population of these levels in different nuclear reactions can be used as a test of nuclear reaction theory as was proposed recently in [41].

V. SUMMARY

The energies and level widths of the first four states in ^{16}F were measured with a ^{15}O beam and proton elastic resonance scattering using the thick target inverse kinematics technique at 180° c.m. This study was made possible by the newly developed ^{15}O radioactive ion beam using BEARS at the 88-Inch Cyclotron. The experimental data were analyzed with R-matrix calculations, and then compared to previous experimental results and theoretical predictions. This $p(^{15}\mathrm{O},p)$ experiment allows us to report more precise level widths than

TABLE III. Comparison of ^{16}F experimental results with the isobaric analog states in ^{16}N and with theoretical calculations in the framework of the potential model.

^{16}N			^{16}F			^{16}F theory			
E_x [MeV]	J^π	C^2S[a]	E_x [MeV ± keV]	J^π	Γ_p [keV][b]	Parameter set #1 (a = 0.65 fm) Γ_{sp} [keV]	Parameter set #2 (a = 0.75 fm) Γ_{sp} [keV]	C^2S (Exp.)	C^2S (Shift)
0.120	0^-	0.95	0	0^-	22.8 ± 14.4	21.8	22	1.04	0.91
0.397	1^-	0.96	0.187 ± 18	1^-	103 ± 12	89.5	96	1.07	0.88
0	2^-	0.93	0.416 ± 20	2^-	4.0 ± 2.5	3.6	4.3	0.93	
0.296	3^-	0.87	0.722 ± 16	3^-	15.1 ± 6.7	12.7	15.0	1.01	

[a]OXBASH calculation reported in Ref. [36].
[b]This work. 95% confidence level.

previously known values, and our experimental results also show very good agreement with theory.

ACKNOWLEDGMENTS

This work was supported by the U.S. Department of Energy, Office of Nuclear Physics, under Contract No. DE-AC02-05CH11231 (Lawrence Berkeley National Laboratory). The authors also appreciate support by the U.S. Department of Energy Grant Nos. DE-FG02-93ER40773 and DE-FG52-06NA26207/A000. The authors would like to thank Mitch Andre Garcia for assistance with the experiment and Christopher Ramsey for his contributions at the medical cyclotron.

[1] D. R. Tilley *et al*., Nucl. Phys. **A564**, 1 (1993).
[2] C. D. Zafiratos *et al*., Phys. Rev. **137**, B1479 (1965).
[3] W. Bohne *et al*., Phys. Lett. **B47**, 342 (1973).
[4] T. Otsubo *et al*., Nucl. Phys. **A259**, 452 (1976).
[5] R. H. Pehl and J. Cerny, Phys. Lett. **14**, 147 (1965).
[6] H. Nann, W. Benenson, E. Kashy, H. P. Morsch, and D. Mueller, Phys. Rev. C **16**, 1684 (1977).
[7] W. A. Sterrenburg *et al*., Nucl. Phys. **A420**, 257 (1984).
[8] H. Fujita *et al*., RCNP Annual Report, 5 (2002).
[9] C. E. Moss and A. B. Comiter, Nucl. Phys. **A178**, 241 (1971).
[10] A. Fazely *et al*., Phys. Rev. C **25**, 1760 (1982).
[11] H. Orihara, S. Nishihara, K. Furukawa, T. Nakagawa, K. Maeda, K. Miura, and H. Ohnuma, Phys. Rev. Lett. **49**, 1318 (1982).
[12] H. Ohnuma *et al*., Nucl. Phys. **A467**, 61 (1987).
[13] R. Madey *et al*., Phys. Rev. C **56**, 3210 (1997).
[14] H. T. Fortune, Phys. Rev. C **52**, 2261 (1995).
[15] K. Ogawa *et al*., Phys. Lett. **B464**, 157 (1999).
[16] J. Powell *et al*., Nucl. Instrum. Methods A **455**, 452 (2000).
[17] J. Powell *et al*., Nucl. Instrum. Methods B **204**, 440 (2003).
[18] F. Q. Guo *et al*., Phys. Rev. C **72**, 034312 (2005).
[19] K. P. Artemov *et al*., Sov. J. Nucl. Phys. **52**, 408 (1990).
[20] T. Delbar *et al*., Nucl. Phys. **A542**, 263 (1992).
[21] K. Peräjärvi *et al*., Phys. Rev. C **74**, 024306 (2006).
[22] J. Powell and J. P. O'Neil, Appl. Radiat. Isot. **64**, 755 (2006).
[23] K. Markenroth *et al*., Phys. Rev. C **62**, 034308 (2000).
[24] J. F. Ziegler, The Stopping and Range of Ions in Matter (SRIM-2003), http://www.srim.org.
[25] J. Moss and G. C. Ball, Lawrence Radiation Laboratory Report, UCRL-17124 (1966).
[26] F. B. Hagedorn, Phys. Rev. **108**, 735 (1957).
[27] S. Bashkin *et al*., Phys. Rev. **114**, 1543 (1959).
[28] G. Dearnaley *et al*., Phys. Lett. **1**, 269 (1962).
[29] S. E. Darden *et al*., Nucl. Phys. **A429**, 218 (1984).
[30] S. Kubono, Nucl. Phys. **A693**, 221 (2001).
[31] T. Teranishi *et al*., Phys. Lett. **B556**, 27 (2003).
[32] A. M. Lane and R. G. Thomas, Rev. Mod. Phys. **30**, 257 (1958).
[33] C. Ruiz *et al*., Phys. Rev. C **71**, 025802 (2005).
[34] F. James and M. Roos, Comput. Phys. Commun. **10**, 343 (1975).
[35] V. Z. Goldberg *et al*., Phys. Rev. C **69**, 031302(R) (2004).
[36] W. Bohne *et al*., Nucl. Phys. **A196**, 41 (1972).
[37] J. Meissner, H. Schatz, H. Herndl, M. Wiescher, H. Beer, and F. Kappeler, Phys. Rev. C **53**, 977 (1996).
[38] R. G. Thomas, Phys. Rev. **81**, 148 (1951).
[39] J. B. Ehrman, Phys. Rev. **81**, 412 (1951).
[40] J. A. Nolen and J. P. Schiffer, Annu. Rev. Nucl. Sci. **19**, 471 (1969).
[41] A. M. Mukhamedzhanov and F. M. Nunes, Phys. Rev. C **72**, 017602 (2005).